Elsevier Editorial System(tm) for Journal of Materials Processing Technology
Manuscript Draft

Manuscript Number: PROTEC-D-12-00022R1

Title: A computational fluid dynamic analysis of the effect of side draughts and nozzle diameter on shielding gas coverage during gas metal arc welding

Article Type: Research Paper

Keywords: CFD, GMAW, welding nozzle diameter, shielding gas coverage, side

Corresponding Author: Miss Gemma Ramsey,

Corresponding Author's Institution: University of Strathclyde

First Author: Gemma Ramsey

Order of Authors: Gemma Ramsey; Alex M Galloway, B.Sc, PhD, CEng; Stuart W Campbell, MEng; Norrie A McPherson; Tom J Scanlon, BEng, PhD, CEng

Abstract: Extensive experimental trials were conducted, emulating the conditions modelled, in order to validate the computational fluid dynamic results. Final results demonstrated that a more constricted nozzle was more effective at creating a stable gas column when subjected to side draughts. Higher shielding gas flow rates further reduce the gas column's vulnerability to side draughts and thus create a more stable coverage. The results have highlighted potential economic benefits for draught free environments, in which, the shielding gas flow rate can effectively be reduced.

Cover Letter

Department of Mechanical and Aerospace Engineering
75 Montrose Street
University of Strathclyde
Glasgow
G1 1XJ

Dear Editors,

I would like to take this opportunity to thank you for considering this paper as it is my first to be submitted for publication. The subject of which is a study of shielding gas composition with respect to side draughts and nozzle diameter. I can conform that this submission is original and has not been submitted for publication anywhere else.

I would like to draw your attention to the close correlation between the computational and experimental validation results and point out that the simplification of the welding arc during computational simulation appears to have a minimal effect on these results.

I look forward to hearing from you in the near future.

Yours faithfully,

Gemma Ramsey

Miss Gemma Ramsey
Department of Mechanical and Aerospace Engineering

12/03/12

The Editor
Journal of Materials Processing Technology

Journal Submission

A computational fluid dynamic analysis of the effect of side draughts and nozzle diameter on shielding gas coverage during gas metal arc welding

Reviewer #1
I appreciate you taking the time to read and comment on this text.

Subject Editor
Many thanks for taking the time to read and comment on this manuscript. I have the pleasure of submitting the amended document for your re-consideration. I have identified the modifications you have suggested and have made the following changes to the script.

Abstract:
I understand your comments regarding the first statement and it has been removed in order to avoid the repetition of the title of the paper. Similarly, line 4 has also been removed and the subsequent statement reworded. The phrase 'as expected' has also been removed from the text.

After reviewing the manuscript, I concur that the final statement of the abstract is out of place and has also been removed.

Main Text:
I have amended the 'Conclusion' section of the manuscript to read 'Conclusions' as you suggested.

I have reconsidered the final paragraph of the conclusions section and, taking into account the JMPT is only reporting on past research, have removed this small ending segment from the paper. I feel the conclusions read better without the statement.

Yours faithfully,

Miss Gemma Ramsey

Highlights

- A simplified computational model and experimental trials correlate closely
- A 16 mm nozzle can produce highly concentrated shielding gas columns with diameters of up to 28 mm
- Decrease in shielding gas coverage and weld quality as side draught velocity increases
- Reduction in nozzle diameter increases the shielding gas columns resistance to side draughts
- Critical ratio of shielding gas to side draught velocity decreases as nozzle diameter decreases

A computational fluid dynamic analysis of the effect of side draughts and nozzle diameter on shielding gas coverage during gas metal arc welding

Ramsey, G.M.[1*], Galloway, A.M.[1], Campbell, S.W.[1] and McPherson, N.A.[2], Scanlon, T.J.[1]

[1] Department of Mechanical & Aerospace Engineering, University of Strathclyde, Scotland, United Kingdom

[2] BAE Systems Surface Ships Limited, Glasgow, United Kingdom

[*]gemma.ramsey@strath.ac.uk

Abstract: Extensive experimental trials were conducted, emulating the conditions modelled, in order to validate the computational fluid dynamic results. Final results demonstrated that a more constricted nozzle was more effective at creating a stable gas column when subjected to side draughts. Higher shielding gas flow rates further reduce the gas column's vulnerability to side draughts and thus create a more stable coverage. The results have highlighted potential economic benefits for draught free environments, in which, the shielding gas flow rate can effectively be reduced.

Keywords: CFD, GMAW, welding nozzle diameter, shielding gas coverage, side draughts

LIST OF SYMBOLS

k	turbulence kinetic energy
ε	rate of dissipation
μ	viscosity
μ_t	turbulent viscosity
G_k	generation of turbulence kinetic energy due to mean velocity gradients
G_b	generation of turbulence kinetic energy due to buoyancy
Y_M	contribution of the fluctuating dilation in compressible turbulence to the overall dissipation rate
σ_k	turbulent Prandtl number for turbulence kinetic energy
σ_ε	turbulent Prandtl number for rate of dissipation
β	thermal expansion coefficient
α	thermal diffusivity

ν	kinematic viscosity
ρ	density
g	gravity
q	heat flux
q_{rad}	radiative heat flux
h_f	fluid-side local heat transfer coefficient
h_{ext}	external heat transfer coefficient
T_w	wall surface temperature
T_f	local fluid temperature
T_{ext}	external heat sink temperature
T_∞	temperature of radiation source or sink
ε_{ext}	emissivity of the external wall surface
σ	Stefan-Boltzmann constant
a_P	centre coefficient
a_{nb}	influence coefficient for neighbouring cells
b	contribution of the constant part of the source term and boundary conditions
P_o	total pressure
P_s	static pressure
S_k, S_ε	user defined source terms
$C_{1\varepsilon}$, $C_{2\varepsilon}$, $C_{3\varepsilon}$,	constants
C_μ	constant
ϕ	general variable

INTRODUCTION

The shielding gas is a fundamental component in any gas shielded welding process and, as a result of individual gas properties, has the ability to significantly influence the appearance and overall weld quality as demonstrated by Vaidya's (2002) in depth analysis of the effect of shielding gas mixtures for semi-automatic welds. The primary purpose of any welding shielding gas is to protect the molten metal during the arc transfer process and to protect the weld surface from reacting with atmospheric contaminants during solidification. This is shown in Tani et al. (2007) through their work investigating the effects of shielding gas in hybrid laser-MIG welding. In each case, the absence of sufficient quantities of shielding gas will generally result in the formation of porosity and other defects in the solidified weld and therefore compromise the quality and integrity of the weld.

Shielding gases are commonly delivered to the welding region in a premixed state in order to take advantage of the beneficial properties of each gas. Argon-based mixed gases are generally used as the preferred shielding gas in cases where carbon steels are welded using the GMAW process. An argon/carbon dioxide (80/20) mixture is a commonly used GMAW shielding gas in Western Europe, particularly in carbon steel fabrication industries. In such cases, carbon dioxide is routinely added to an argon-based mixture as it has the ability to stabilize the arc and produce a more consistent weld than argon on its own as demonstrated by Chae et al. (2008).

The correct shielding gas flow rate can vary considerably and is dependant upon the welding process, welding orientation, operating parameters and shielding gas composition. Typically,

GMAW shielding gas flow rates are in the region 15-20 l/min, although Campbell et al (Under review) have found that this can be lowered considerably with a flow rate of 6 l/min producing good quality welds in a draught free environment. It is common for flow rates to be set in excess of 25 l/min, normally because the welder makes the assumption that more gas means better protection. However, other studies namely Uttrachi (2007) and Loxton Industries (2010) have explored the impact of the initial surge of shielding gas, at weld ignition, has on the stability of the shielding gas column. This effect has been reported to create turbulence in the flow, which, in turn draws atmospheric gases into the weld region potentially creating defects within the solidified weld. Lyttle and Stapon (2005) have shown this to also be the case after the initial surge with flow rates above approximately 23 l/min creating turbulence within the shielding gas column.

Side draughts present a significant problem to the welding process from both a technical and economic viewpoint, potentially adversely affecting the shielding gas's ability to protect the weld region from contamination by atmospheric gases such as nitrogen and oxygen. To counteract these effects, there is a generally accepted industrial mindset that more must be better, and for that reason shielding gas flow rates in the region of 20-25 l/min are typically used when draughts are present; however there is no scientific evidence to support this action.

Very little published work is available on the specific subject of the application of CFD modelling to weld shielding gas coverage. A finite element model of a GMAW welding nozzle was developed by Dreher et al. (2009) (2010) using ANSYS CFX to analyse the effects of turbulence in the gas distribution, finding that turbulence significantly affects conditions at the

work piece. However, there is no literature at present reporting on the use of CFD to model the problem of side draughts during the GMAW process. The development of this tool could potentially be of major benefit and, would allow the simulation of potential welding environments to be evaluated without the need to consistently resort to expensive, time consuming and often-inconclusive plant trails.

MODEL

The present study investigated the effect that the shielding gas flow rate, side draught velocity and nozzle outlet diameter have on the shielding gas flow characteristics during GMAW through the use of CFD modelling. A multi-physics, 3D transient state model was therefore developed for three different welding torch nozzle diameters using the CFD software Fluent. In order to validate the CFD model, extensive experimental trials were conducted which replicated the geometry and welding conditions simulated.

The model geometry was constructed in Gambit, in which, the welding nozzle is positioned with a 10 mm gap directly above the surface of a 250 x 500 x 8 mm thick plate. The nozzle and plate are situated within a defined volume of sufficient size to ensure that all flow development was captured, although the main area of interest which was the 10 mm between the tip of the nozzle and the plate surface. Fig.1 shows a 12 mm diameter hemisphere positioned directly below the nozzle which was used to represent the welding arc region. Boundary layers and zones were defined within the geometry of the model, enabling conditions for each to be set in Fluent. Finally, the model was then meshed using tetrahedral elements.

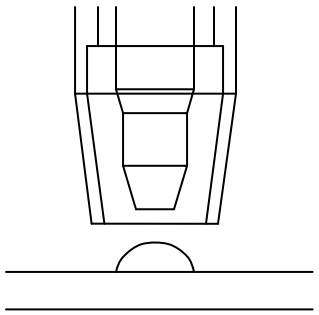

Fig.1: Nozzle and arc geometry in Gambit

The generated mesh was then imported into Fluent, where the physics of the model were defined. The energy equation was initiated allowing heat transfer through the fluid and plate to be analysed. A combined convection and external radiation condition was used to model the heat transfer from the welding arc to the plate using Equation. 1.

$$q = h_f (T_w - T_f) + q_{rad} = h_{ext} (T_{ext} - T_w) + \varepsilon_{ext} \sigma (T_\infty^4 - T_w^4) \quad \text{..... (1)}$$

The gravitational acceleration components were input enabling buoyancy effects to be considered. The buoyancy forces were evaluated using Equation.2, a ratio of the Grashof and Reynolds numbers.

$$\frac{GR}{\mathrm{Re}^2} = \frac{g\beta\Delta TL}{\nu^2} \quad \text{..... (2)}$$

Buoyancy contributed strongly to the flow when the ratio in Equation.2 approached unity.

Semi-empirical transport equations (Equation.3 & 4) for the standard k-ε turbulence model were used to evaluate the turbulent kinetic energy of the flow and its rate of dissipation.

$$\frac{\partial}{\partial t}(\rho k)+\frac{\partial}{\partial x_i}(\rho k v_i)=\frac{\partial}{\partial x_j}\left[\left(\mu+\frac{\mu_t}{\sigma_k}\right)\frac{\partial k}{\partial x_j}\right]+G_k+G_b-\rho\varepsilon-Y_M+S_k \quad \text{..... (3)}$$

$$\frac{\partial}{\partial t}(\rho \varepsilon)+\frac{\partial}{\partial x_i}(\rho \varepsilon v_i)=\frac{\partial}{\partial x_j}\left[\left(\mu+\frac{\mu_t}{\sigma_\varepsilon}\right)\frac{\partial \varepsilon}{\partial x_j}\right]+C_{1\varepsilon}\frac{\varepsilon}{k}(G_k+C_{3\varepsilon}G_b)-C_{2\varepsilon}\rho\frac{\varepsilon^2}{k}+S_\varepsilon \quad \text{..... (4)}$$

The turbulent viscosity was determined by combining the turbulent kinetic energy and the rate of dissipation as shown in Equation.5.

$$\mu_t=\rho C_\mu\frac{k^2}{\varepsilon} \quad \text{..... (5)}$$

The side draught was modelled as a uniform laminar flow, as this best represented the experimental validation, by defining a pressure inlet within the fluid volume. This causes a pressure difference in the model and a stream of air to flow from the pressure inlet to the nozzle. The streams velocity was related to the total and static pressures through Bernoulli's equation (Equation.6).

$$p_0=p_s+\frac{1}{2}\rho v^2 \quad \text{..... (6)}$$

The desired side draught velocities were generated by adjusting the total pressure. Shielding gas flow rates of 5, 10, 15 and 18 l/min through nozzle diameters of 11, 14 and 16 mm were simulated with 0-8 mph side draughts, with 1 mph increments.

The shielding gas used during this work was 80%Ar/20%CO_2, the properties of which were defined by importing the individual properties of argon and carbon dioxide from Fluent's material property database, specifying their respective ratios and applying the rule of mixtures. These properties are shown in Table 1 and vary with temperature according to a defined polynomial function. A mass flow inlet condition positioned inside the nozzle allowed the flow rate of the shielding gas to be set.

Property	**Argon**	**Carbon Dioxide**	**80%Ar20%CO_2 Mixture**
Density (kg/m^3)	1.6228	1.7878	Ideal Gas
Cp (J/kgK)	520.64	840.37	Mixing law
Thermal Conductivity (W/mK)	0.0158	0.0145	0.0454
Viscosity (kg/ms)	2.125e-5	1.37e-5	1.72e-5
Molecular Weight (kg/kgmol)	39.948	44.00995	2.88e-5

Table 1: The required properties of Argon, Carbon Dioxide and the resulting mixture

Jönsson et al. (1995) determined that the peak arc temperature during GMAW using a pure argon shielding gas was approximately 24,000 K. To ensure that the correct arc temperature was fed into the model, the heat transfer through the plate was found experimentally using K-type thermocouples to establish the temperature distribution. The results from this were confirmed through thermal imaging measurements. The arc temperature was then systematically increased in Fluent until the correct heat transfer from arc to plate was achieved in the model. This occurred at a value of 32,000 K, higher than that determined by Jönsson et al. However this was expected given a shielding gas mixture of 80%Ar/20%CO_2 was used and CO_2 is known to

produce greater penetration as shown by Chae et al. (2008). It was therefore anticipated that greater penetration would be the result of an increased arc temperature when compared to that of pure argon.

An interface was defined between the fluid and plate volumes enabling Fluent to compute across this boundary as their respective meshes slide over one another. Finally, the convergence criteria of the simulations were set. Following each iteration, the residual sum (Equation.7) for each variable is computed, which ideally, will tend to zero as the solution converges. In reality, they reduce to a small value and then become constant.

$$a_P \phi_P = \sum_{nb} a_{nb} \phi_{nb} + b \quad \text{.......} \quad (7)$$

Equation.7 shows the conservation equation after discretisation for a variable ϕ at a cell P that is then summated over all cells. The model was considered to have solved when each residual simultaneously converged to a value of 1e-5.

EXPERIMENTAL VALIDATION

An integral part of this research involved experimentally validating the CFD model results through extensive trials emulating to the conditions simulated. The experimental validation took place in the form of bead on plate welds on 8 mm thick DH36 steel.

Trials were performed on an automatic welding rig that moved the plate at a pre-set velocity of 3.2 mm/s beneath a stationary GMAW nozzle. The nozzle was positioned with a 10 mm gap, centrally located above a 250 x 500 mm plate. The shielding gas used throughout the experimentation was 80%Ar/20%CO_2.

A pre-calibrated portable arc monitoring system was used throughout the experimentation in order to accurately measure the arc current and voltage, whilst a second welding monitor was implemented to measure the shielding gas flow rate; the experimental trials considered shielding gas flow rates of 5, 10, 15 and 18 l/min. The average welding parameters used throughout were an arc current and voltage of 210 A and 24.6 V respectively. A flow device capable of producing a constant laminar stream of air was used to produce a side draught at a consistent velocity. The velocity of the draught was measured using a pre-calibrated hot-wire anemometer in the region between the welding nozzle and the plate. The welding region was subjected to side draught velocities of 0-8 mph, in 1 mph increments. As in the CFD model, experimental data was also generated for constricted nozzles of diameter 11, 14 and 16 mm. Thermal data was generated through the use of K-type thermocouples and thermal imaging, enabling a clear view of the temperature distribution throughout the plate to be established.

The weld quality was evaluated through a combination of visual and X-ray inspection; the latter being graded according to the level of porosity present. The X-Ray inspection results are shown in Tables 2(a-c) where green indicates a pass, yellow indicates dispersed porosity and red indicates a highly porous weld. Figures 2a and 2b show the typical radiographic images from a pass weld and a highly porous weld.

(a) 16 mm	Side Draught Velocity (mph)								
Gas Flow (l/min)		0	1	2	3	4	5	6	7	8
	5									
	10									
	15									
	18									
(b) 14 mm	Side Draught Velocity (mph)								
Gas Flow (l/min)		0	1	2	3	4	5	6	7	8
	5									
	10									
	15									
	18									
(c) 11 mm	Side Draught Velocity (mph)								
Gas Flow (l/min)		0	1	2	3	4	5	6	7	8
	5									
	10									
	15									
	18									

Table 2a, b and c: Grading of X-Ray inspections for 16, 14 and 11 mm

Fig. 2a: An X-Ray image of a clear weld

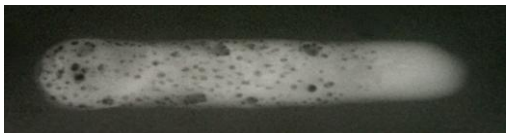

Fig. 2b: An X-Ray image of a highly porous weld

RESULTS

Each model was subjected to a series of simulations using the unsteady solver consisting of each gas flow rate evaluated at each side draught, a total of 32 simulations per nozzle. The results were evaluated using contour plots of mass concentration of argon; since the shielding gas modelled was 80 % argon and 20 % carbon dioxide, this meant that a contour of 80 % argon was

equal to 100 % shielding gas. Fig.3 is a contour plot showing mass concentration of argon for a 16mm nozzle with a shielding gas flow rate of 15 l/min and no side draught. In this instance the shielding gas achieves a 26 mm diameter column of coverage over the weld. This was measured by scaling the shielding gas contour plots to actual size enabling the shielding gas column diameter to be measured directly from the plot as shown in Fig. 3. Tables 3(a-c) show the diameter of shielding gas coverage for the 16 mm, 14 mm and 11 mm nozzles respectively and refer to the diameter (mm) over which 100 % shielding gas is present.

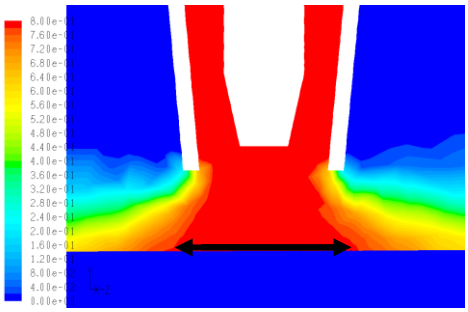

Fig.3: Contour plot of mass concentration of argon with 26 mm of 100 % coverage

(a) 16mm	Side Draught Speed (mph)								
Gas Flow (l/min)		0	1	2	3	4	5	6	7	8
	5	28	22	18	0	0	0	0	0	0
	10	26	24.8	22	18	14	0	0	0	0
	15	26	26	24	21.6	20	16	6	0	0
	18	26	26	26	22	21.2	18	14	2	0
(b) 14mm	Side Draught Speed (mph)									
Gas Flow (l/min)		0	1	2	3	4	5	6	7	8
	5	26.8	26.8	22	17.2	12	0	0	0	0
	10	26	25.2	23.2	20.8	20	18	14.4	6.8	2
	15	23.6	23.6	23.6	22	21.2	20	18.4	17.6	16
	18	22.8	22.8	22.8	22	21.2	20	19.2	18	18
(c) 11mm	Side Draught Speed mph)									
Gas Flow (l/min)		0	1	2	3	4	5	6	7	8
	5	26.4	26.4	22	18.4	17.2	10.8	0	0	0
	10	25.2	25.2	24.4	22	21.6	20.4	18.8	17.6	15.6
	15	23.2	23.2	23.2	22.4	22.4	22	20.8	20.8	20.4
	18	22.8	22.8	22.8	22.8	22.4	22	21.6	21.6	21.6

Table 3a, b and c: The diameter (mm) and classification of shielding gas coverage for 16, 14 and 11 mm nozzles

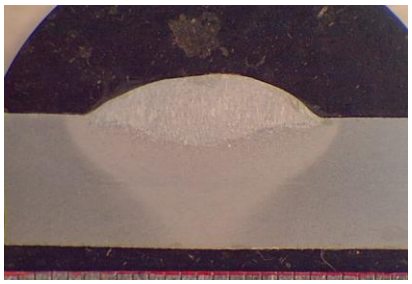

Fig.4: A weld cross-section showing width and penetration

A weld macrograph was produced for a section of weld generated in the experimental trials as shown in Fig.4; the weld width (15 mm) was then used for the generation of a grading system, which was subsequently applied to the CFD results. All gas columns of diameter 15 mm and above were classified as good coverage (green), between 10-15 mm coverage was reduced quality coverage (yellow) and below 10 mm coverage was of poor quality (red).

The model presented good welds to have the shielding gases 100 % coverage centred directly below the nozzle. As the draught velocity was increased the 100 % coverage decreases and drifts off centre exposing one side of the weld as shown in Fig. 5(a-f). Eventually, the side draught becomes strong enough to prevent adequate coverage occurring. The side draught velocity at which this occurs increases as nozzle diameter decreases.

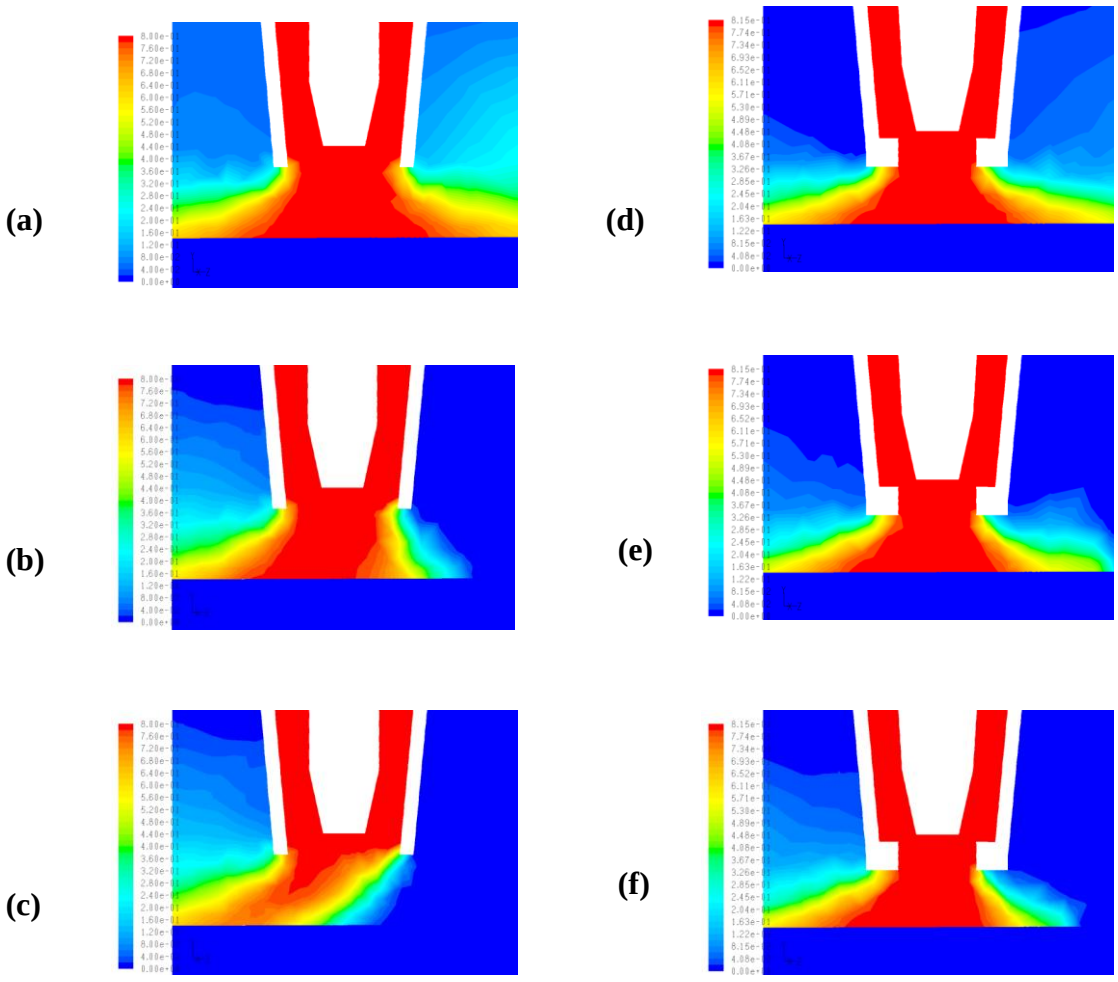

Fig.5 A comparison of 16 mm nozzle gas columns to 11 mm nozzle gas columns.
(a) 16 mm nozzle at 15 l/min shielding gas flow with a 1 mph side draught
(b) 16 mm nozzle at 15 l/min shielding gas flow with a 5 mph side draught
(c) 16 mm nozzle at 15 l/min shielding gas flow with an 8 mph side draught
(d) 11 mm nozzle at 15 l/min shielding gas flow with a 1 mph side draught
(e) 11 mm nozzle at 15 l/min shielding gas flow with a 5 mph side draught
(f) 11 mm nozzle at 15 l/min shielding gas flow with an 8 mph side draught

From Table 3a, the 16 mm nozzle results followed a pattern showing that as the gas flow rate was increased, the more resistance the shielding gas column had to side draughts, with the 15 l/min and 18 l/min gas flow rates able to produce good welds up to draughts of 5 mph. From Table 3b, the 14 mm nozzle followed a similar pattern. As with the other diameters, higher gas flow rates from the 11 mm nozzle showed more resistance to side draughts. The 10, 15 and 18 l/min flow rates each managed to withstand all the draughts to produce good welds. Fig.5 compares the results of 1, 5 and 8 mph side draughts on the 16 and 11 mm nozzles.

The change in gas flow distribution as the nozzle diameter decreases is noticeable from Tables 3(a-c). The 11 mm diameter nozzle has been shown to provide the greatest resistance to side draughts of the three nozzle diameters considered. This is due to the principle of the conservation of mass. The smaller the nozzle exit diameter, the higher the velocity of the exiting gas as demonstrated in Fig. 6a and b. The 16 mm nozzle generates up to 5 mph shielding gas velocities through its exit while the 11 mm nozzle generates between 10-18 mph shielding gas velocities.

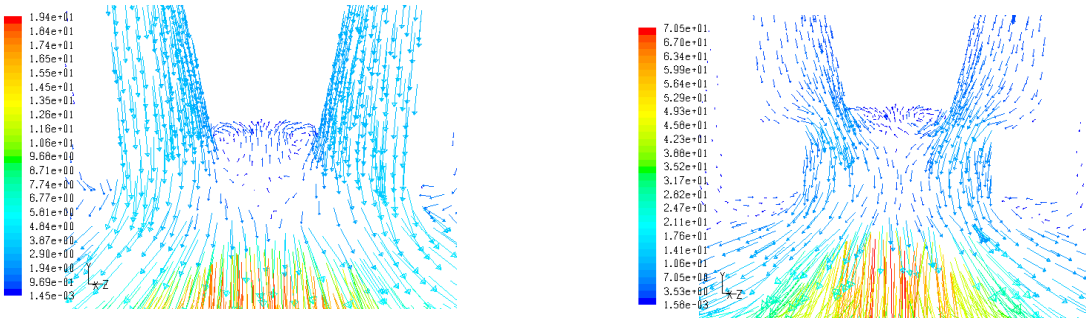

Fig.6a and b: Shielding gas velocities through the 16 mm and 11 mm nozzle exits respectively

The faster the gas exits the nozzle, the greater the draught needed to push it off course. Although the coverage of 22.8 mm, from the 11 mm nozzle at 18 l/min with no draught, is low when compared to the 26 mm coverage the 16 mm nozzle manages, the 11 mm nozzle is able to maintain that level of coverage from 0 to 8 mph. The 16 mm nozzle is more susceptible to the draught and is unable to maintain the same coverage at the same flow rates.

A critical ratio of shielding gas to side draught velocity can be determined, in doing so presenting the pass-fail boundary condition for each nozzle diameter. A ratio of approximately 2-2.5 has been determined for a conventional 16 mm nozzle, whilst ratios of approximately 1.5 and 0.8 for the 14 and 11 mm nozzles respectively. The critical ratio has been shown to decrease in line with the outlet diameter of the nozzle, thus highlighting the effectiveness of the reducing the nozzle diameter.

The results for the experimental validation are shown in Tables 2(a-c). The results follow the same trends identified through the CFD model showing that as the shielding gas flow rate increased the gas columns resistance to side draughts also increased. The results also clearly indicate that the 11 mm nozzle was capable of producing good, clear welds under higher velocities of side draught than the 16 mm nozzle. This finding is significant as it presents the potential to make welding a more efficient process in terms of shielding gas usage, therefore reducing costs and run time.

CONCLUSIONS

A CFD model has been developed to determine the effects of nozzle diameter and side draughts on the shielding gas flow coverage during GMAW. An economic benefit to industry of constricting nozzle diameter has been identified allowing for a lower shielding gas flow rate to be implemented whilst maintaining side draught resistance. The conclusions may be summarised as follows:

1. It was shown that the simplified computational model and experimental trials correlate closely through the use of their respective grading systems. The results show that a good shielding gas coverage as determined in the CFD model translated into a good quality weld determined by X-Ray inspection of the experimental trials.

2. The CFD model has demonstrated the ability of a 16 mm nozzle to produce highly concentrated shielding gas columns with diameters of up to 28 mm. From the experimental trails this can be seen as an excessive amount of coverage. A good quality weld was produced from shielding gas columns as small as 15 mm.

3. Both the CFD model and experimental trials have highlighted the significant effect side draughts have on shielding gas columns and consequently weld quality. As anticipated, there is a progressive decrease in the shielding gas coverage and quality as side draught velocity increases.

4. A reduction in nozzle diameter has been found to increase the shielding gas columns resistance to side draughts. The model predicted that an 11 mm nozzle was capable of maintaining a shielding gas column even at higher side draughts. This was validated through X-Rays of the corresponding experimental trials showing good quality welds.

5. The critical ratio of shielding gas to side draught velocity is shown to decrease with a reduction in the nozzle outlet diameter. This reinforces the effectiveness of reducing the nozzle outlet diameter when subjected to side draughts.

ACKNOWLEDGEMENTS

The author would like to thank BAE Systems for its support and contribution to this work through use of facilities and supplying materials.

ROLE OF THE FUNDING SOURCE

BAE Systems provided the materials required for the practical portion of this study, as well as x-ray analysis facilities. This paper was reviewed by N. McPherson, a BAE Systems engineer who also was an integral part of the decision to submit.

REFERENCES

G. Tani, G. Campana, A. Fortunato, A. Ascari: 'The Influence of Shielding Gas in Hybrid Laser-MIG Welding.*'Applied Surface Science.*, 2007, **253**, 8050-8053.

G.D. Uttrachi, (2007) 'GMAW Shielding Gas Flow Control Systems'. *Welding Journal.,* 2007, **86(4),** 22-23.

H.B. Chae, C.H. Kim, J.H. Kim, S. Rhee: **'**The effect of shielding gas composition in CO_2 laser-gas metal arc hybrid welding.' *IMechE Engineering Manufacture.,* 2008, **222B**, 1315-1324.

K. Lyttle, G. Stapon: 'Simplifying Shielding Gas Selection.' *Practical Welding Today.*, 2005, **9**, No. 1.

Loxton Industries: 'New Welding Gas Innovation'. *Australasian Welding Journal.*, 2010, **55(1)**, 10-11.

M. Dreher, U. Füssel, M. Schnick, M. Hertel: **'**Numerical simulation of the shielding gas flow with GMA welding and options of validation by diagnostics,' *Materials Science and Technology.,* 2009, **2**, 39-49

M. Dreher, U. Füssel, M. Schnick: ‘Numerical optimization of gas metal arc welding torches using ANSYS CFX *Proc*.’ 63rd Annual Assembly and Int. Conf. of the Int. Institute of Welding, Istanbul, Turkey, 11-17 July 2010.

P.G. Jönsson, T.W. Eagar, J. Szekely: **‘**Heat and metal transfer in gas metal arc welding using argon and helium.’ *Metallurgical and Materials Transactions B.*,1995, **26B**, 383-395.

S.W. Campbell, A.M. Galloway, N.A. McPherson: ‘Techno-economic evaluation of reducing shielding gas consumption in GMAW whilst maintaining weld quality.’ *International Journal for Advanced Manufacturing Technology*. Under review.

V.V. Vaidya: **‘**Theory and practice of shielding gas mixtures for semi-automatic welds.’ *Welding Journal.*, 2002, **Dec**, 43-48.

Figure 1

Click here to download high resolution image

Figure 2a

Click here to download high resolution image

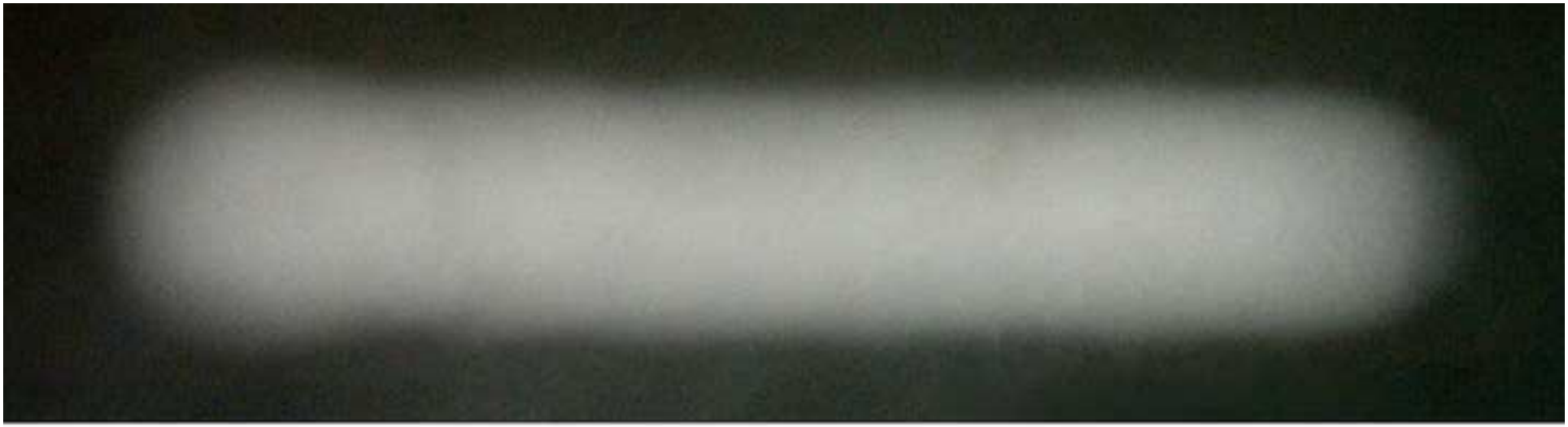

Figure 2b

Click here to download high resolution image

Figure 3

Click here to download high resolution image

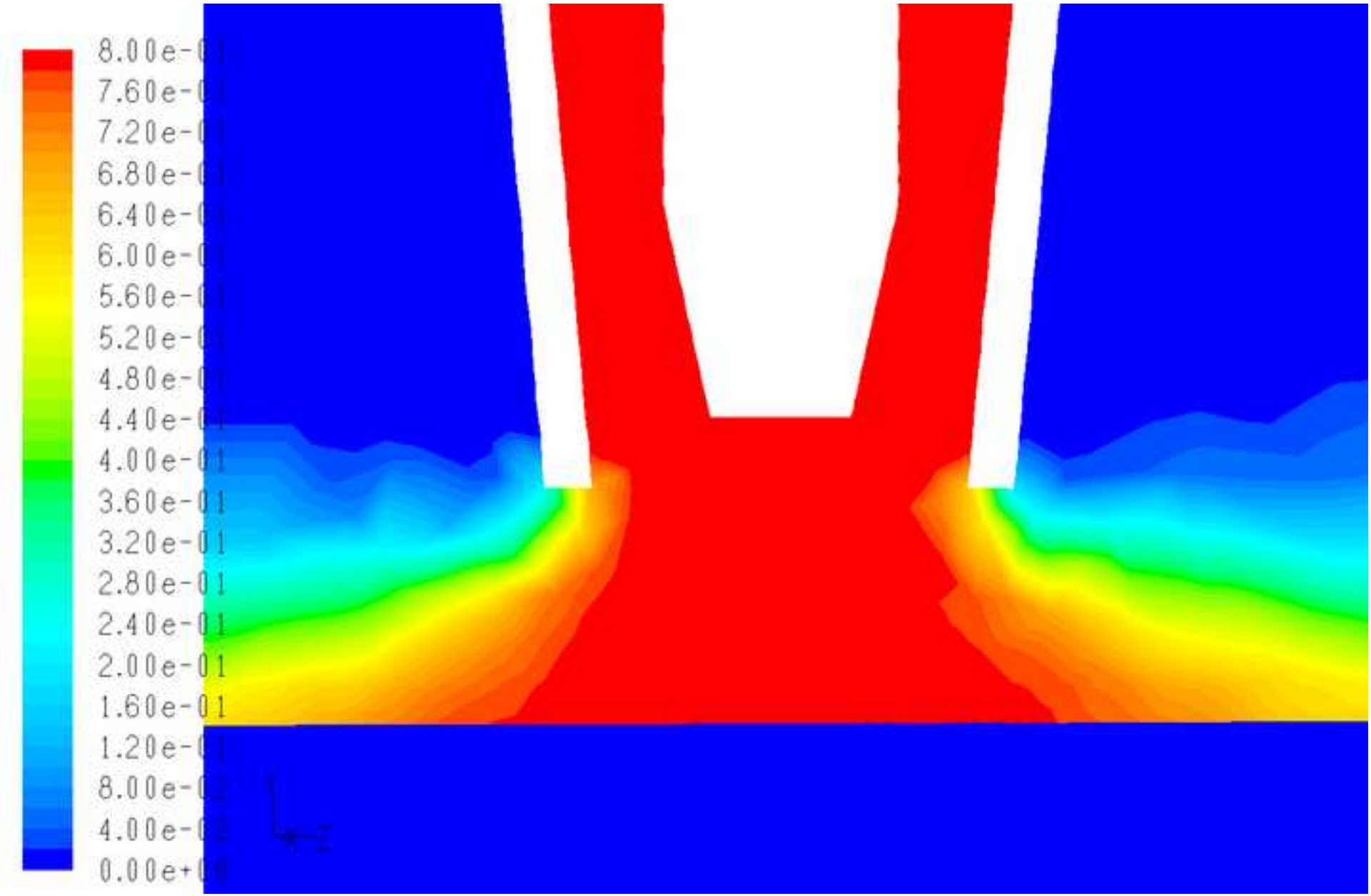

Figure 4

Click here to download high resolution image

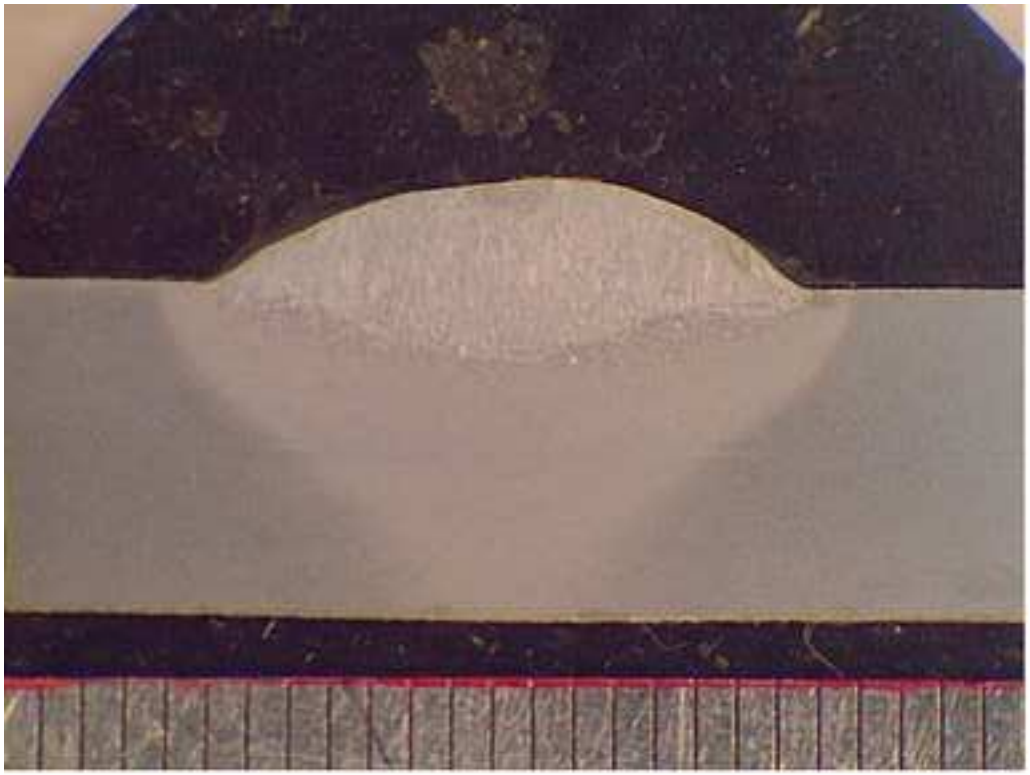

Figure 5a

Click here to download high resolution image

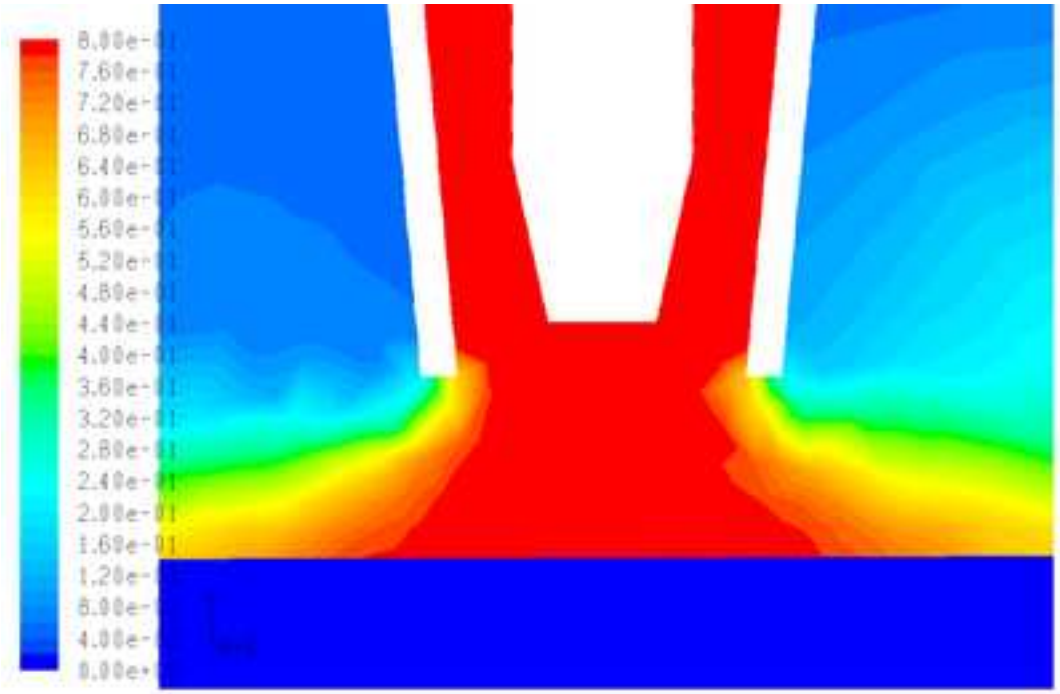

Figure 5b

Click here to download high resolution image

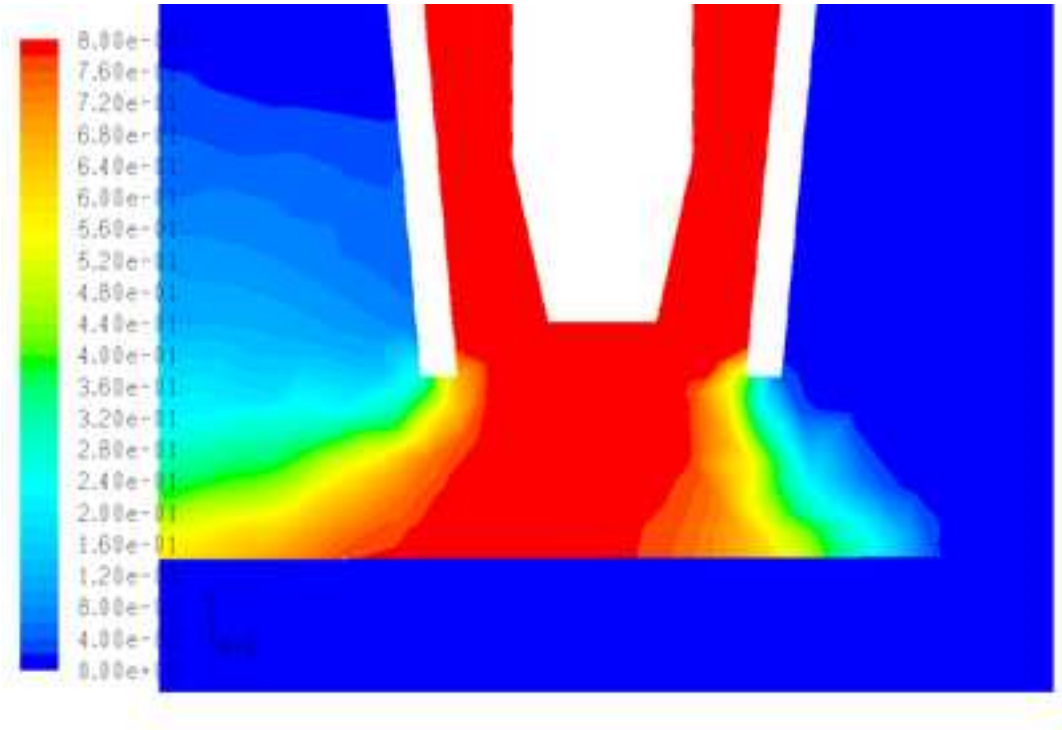

Figure 5c

Click here to download high resolution image

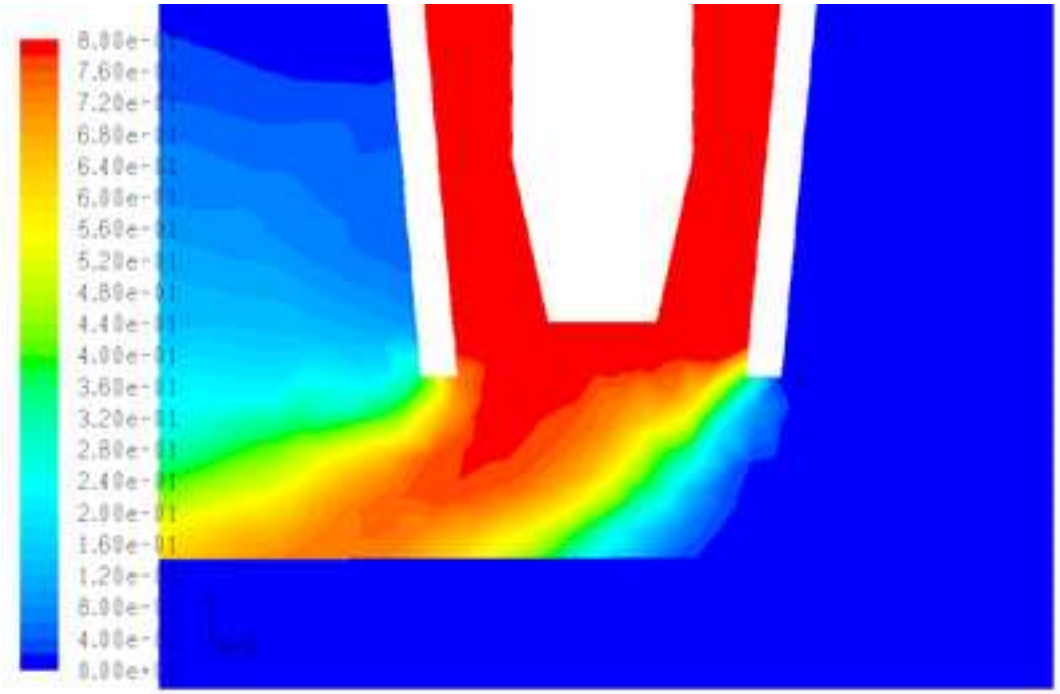

Figure 5d

Click here to download high resolution image

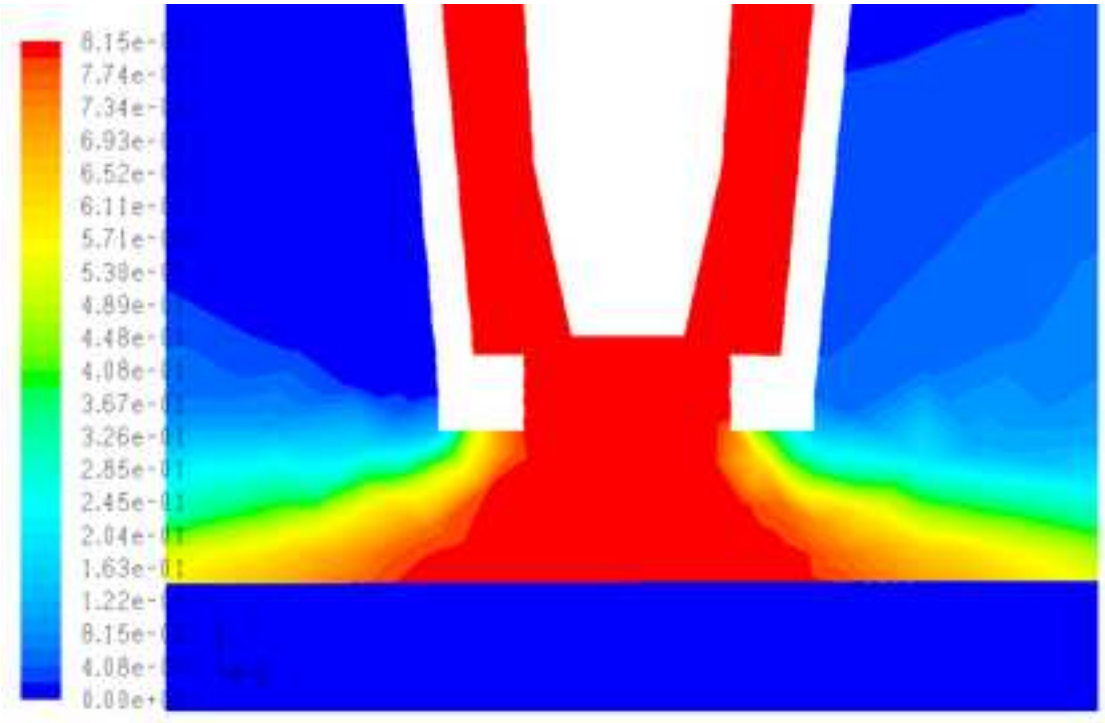

Figure 5e

Click here to download high resolution image

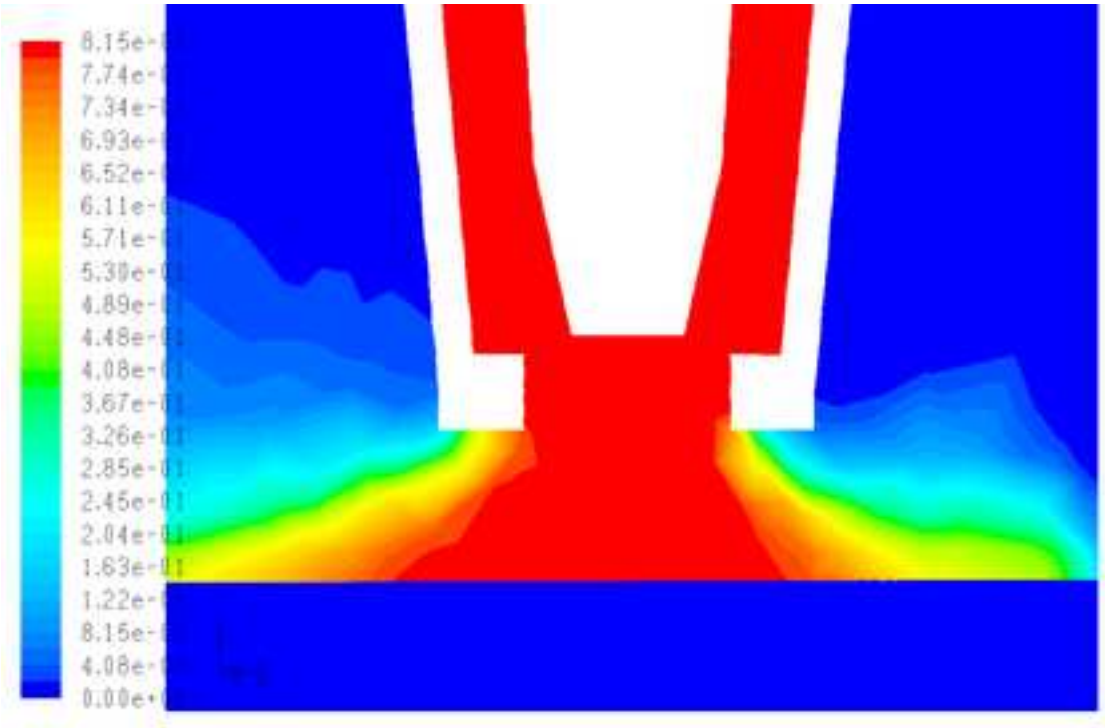

Figure 5f

Click here to download high resolution image

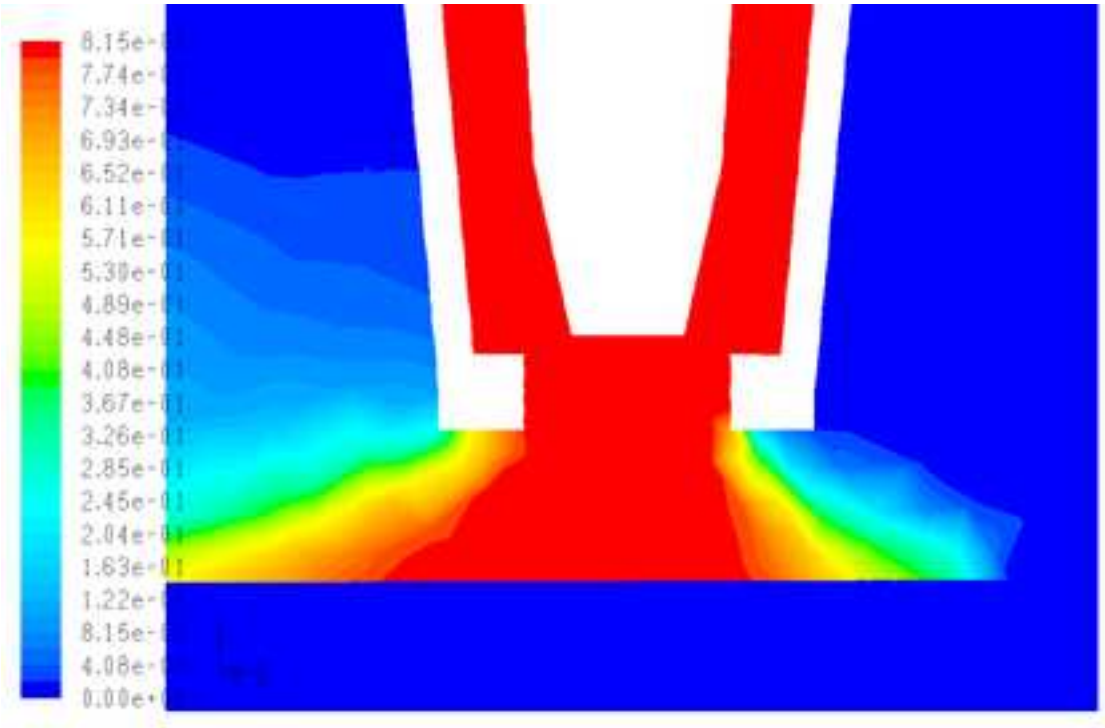

Figure 6a

Click here to download high resolution image

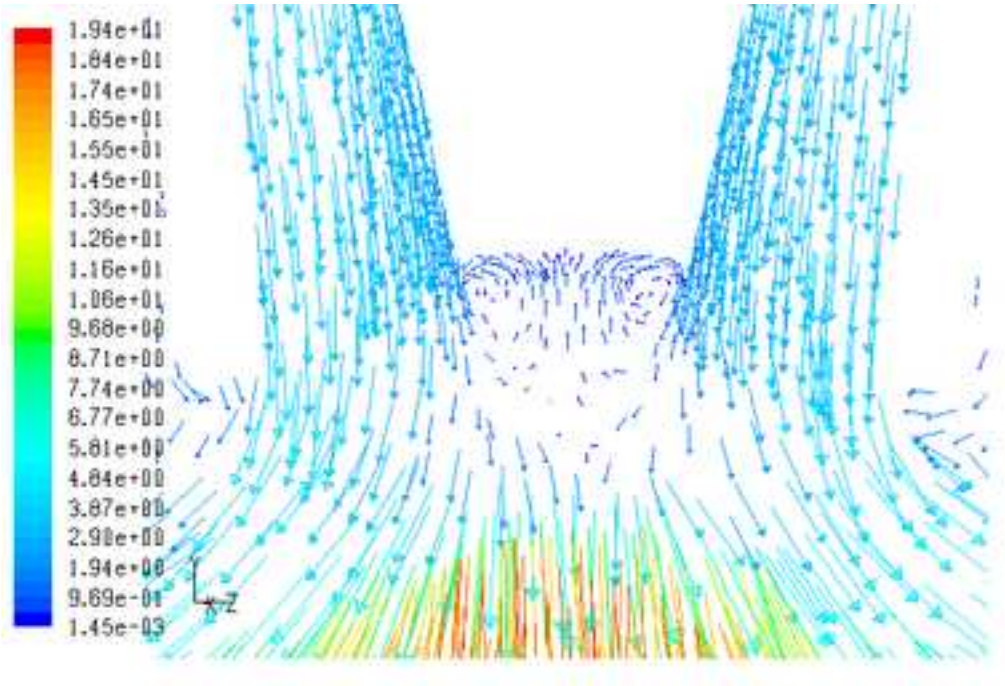

Figure 6b

Click here to download high resolution image

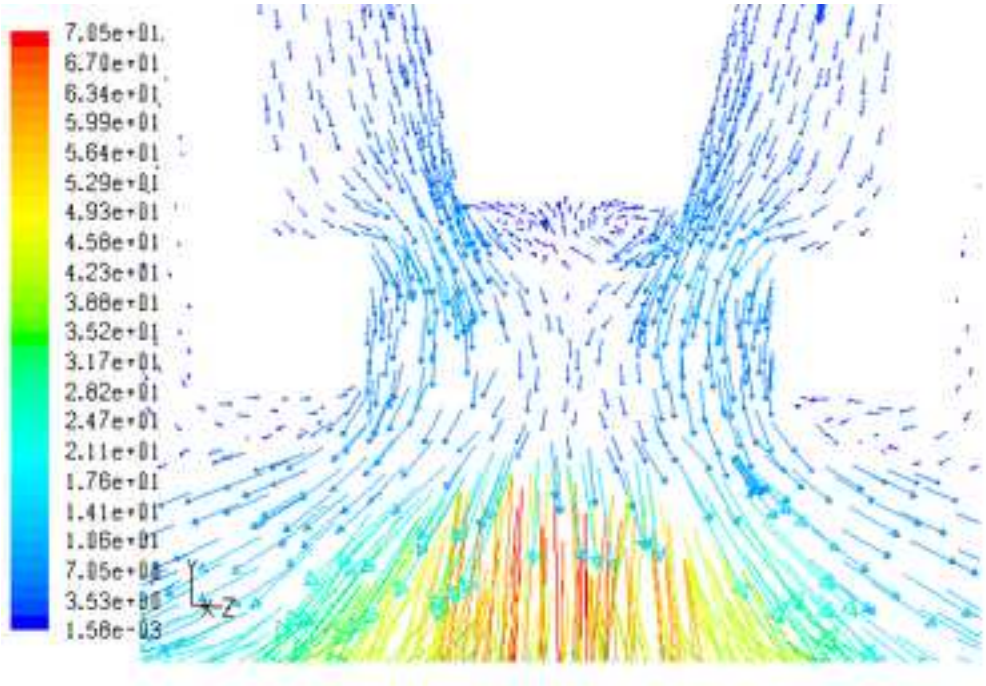

Table 1

Click here to download high resolution image

Property	Argon	Carbon Dioxide	80%Ar20%CO_2 Mixture
Density (kg/m^3)	1.6228	1.7878	Ideal Gas
Cp (J/kgK)	520.64	840.37	Mixing law
Thermal Conductivity (W/mK)	0.0158	0.0145	0.0454
Viscosity (kg/ms)	2.125e-5	1.37e-5	1.72e-5
Molecular Weight (kg/kgmol)	39.948	44.00995	2.88e-5

Table 2

Click here to download high resolution image

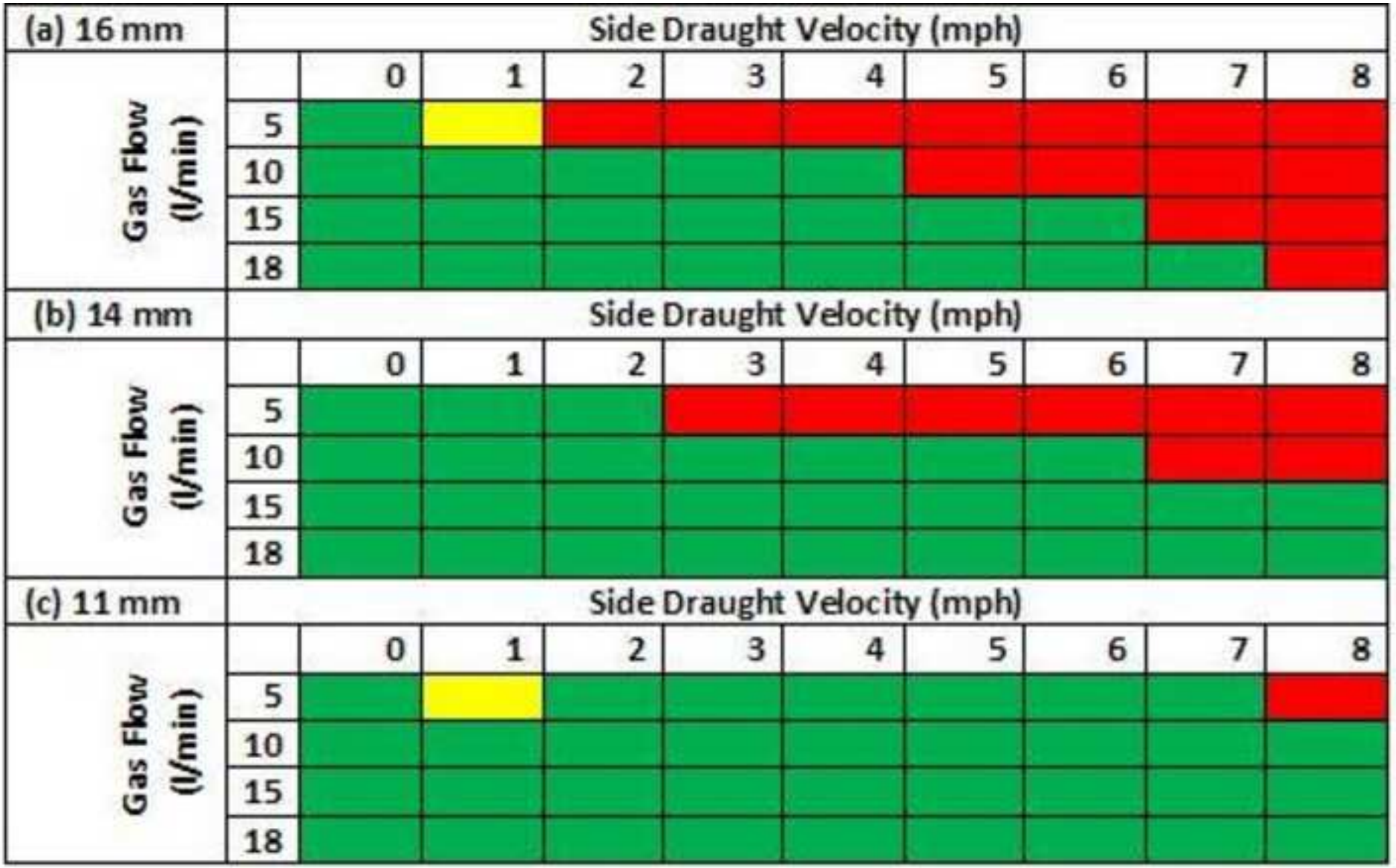

Table 3

Click here to download high resolution image

(a) 16mm	Side Draught Speed (mph)								
Gas Flow (l/min)		0	1	2	3	4	5	6	7	8
	5	28	22	18	0	0	0	0	0	0
	10	26	24.8	22	18	14	0	0	0	0
	15	26	26	24	21.6	20	16	6	0	0
	18	26	26	26	22	21.2	18	14	2	0
(b) 14mm	Side Draught Speed (mph)									
Gas Flow (l/min)		0	1	2	3	4	5	6	7	8
	5	26.8	26.8	22	17.2	12	0	0	0	0
	10	26	25.2	23.2	20.8	20	18	14.4	6.8	2
	15	23.6	23.6	23.6	22	21.2	20	18.4	17.6	16
	18	22.8	22.8	22.8	22	21.2	20	19.2	18	18
(c) 11mm	Side Draught Speed mph)									
Gas Flow (l/inm)		0	1	2	3	4	5	6	7	8
	5	26.4	26.4	22	18.4	17.2	10.8	0	0	0
	10	25.2	25.2	24.4	22	21.6	20.4	18.8	17.6	15.6
	15	23.2	23.2	23.2	22.4	22.4	22	20.8	20.8	20.4
	18	22.8	22.8	22.8	22.8	22.4	22	21.6	21.6	21.6